

A blind deconvolution approach to recover effective connectivity brain networks from resting state fMRI data

Guo-Rong Wu^{a,b}, Wei Liao^c, Sebastiano Stramaglia^d, Ju-Rong Ding^{b,e},
Huafu Chen^b, Daniele Marinazzo^{a,*}

^a*Faculty of Psychology and Educational Sciences, Department of Data Analysis, Ghent University, Henri Dunantlaan 1, B-9000 Ghent, Belgium.*

^b*Key Laboratory for NeuroInformation of Ministry of Education, School of Life Science and Technology, University of Electronic Science and Technology of China, Chengdu 610054, China.*

^c*Center for Cognition and Brain Disorders and the Affiliated Hospital, Hangzhou Normal University, Hangzhou 310015, China.*

^d*Dipartimento di Fisica, Università degli Studi di Bari and INFN, via Orabona 4, 70126 Bari, Italy.*

^e*Department of Psychological and Brain Sciences - Programs in Neuroscience and Cognitive Science, Indiana University, Bloomington, Indiana 47405, USA.*

Abstract

A great improvement to the insight on brain function that we can get from fMRI data can come from effective connectivity analysis, in which the flow of information between even remote brain regions is inferred by the parameters of a predictive dynamical model. As opposed to biologically inspired models, some techniques as Granger causality (GC) are purely data-driven and rely on statistical prediction and temporal precedence. While powerful and widely applicable, this approach could suffer from two main limitations when applied to BOLD fMRI data: confounding effect of hemodynamic response function (HRF) and conditioning to a large number of variables in presence of short time series. For task-related fMRI, neural population dynamics can be captured by modeling signal dynamics with explicit exogenous inputs; for resting-state fMRI on the other hand, the absence of explicit inputs makes this task more difficult, unless relying on some specific prior physiological

*Corresponding author

Email address: `daniele.marinazzo@ugent.be` (Daniele Marinazzo)

hypothesis. In order to overcome these issues and to allow a more general approach, here we present a simple and novel blind-deconvolution technique for BOLD-fMRI signal. In a recent study it has been proposed that relevant information in resting-state fMRI can be obtained by inspecting the discrete events resulting in relatively large amplitude BOLD signal peaks. Following this idea, we consider resting fMRI as 'spontaneous event-related', we individuate point processes corresponding to signal fluctuations with a given signature, extract a region-specific HRF and use it in deconvolution, after following an alignment procedure. Coming to the second limitation, a fully multivariate conditioning with short and noisy data leads to computational problems due to overfitting. Furthermore, conceptual issues arise in presence of redundancy. We thus apply partial conditioning to a limited subset of variables in the framework of information theory, as recently proposed. Mixing these two improvements we compare the differences between BOLD and deconvolved BOLD level effective networks and draw some conclusions. *Keywords:* BOLD signal, Deconvolution, Effective connectivity, Granger causality

1. Introduction

We can learn a lot on the functioning of the human brain in health and disease when we consider it as a large-scale complex network, whose properties can be analyzed using graph theoretical analysis (Bullmore and Sporns, 2009). With the advent of miscellaneous and noninvasive MRI techniques, this *connectome* has been mainly characterized by either structural or functional connectivity. Structural connectivity is commonly based on white matter tracts quantified by diffusion tractography (Hagmann et al., 2008); functional connectivity relies on the other hand on statistical dependencies such as temporal correlation (Salvador et al., 2005). An important addition to this framework can come from effective connectivity analysis (Stephan and Roebroeck, 2012), in which the flow of information between even remote brain regions is inferred by the parameters of a predictive dynamical model.

For some techniques, such as dynamic causal modelling (DCM) and structural equation modelling (Büchel and Friston, 1997; Friston et al., 2003), these models are built and validated from specific anatomical and physiological hypotheses. Other techniques such as Granger causality analysis (GCA)

(Bressler and Seth, 2011), are on the other hand data-driven and rely purely on statistical prediction and temporal precedence. While powerful and widely applicable, this last approach could suffer from two main limitations when applied to blood-oxygenation level-dependent (BOLD)-functional MRI (fMRI) data: confounding effect of hemodynamic response function (HRF) and conditioning to a large number of variables in presence of short time series. Early interpretation of fMRI based directed connectivity by GCA always assumed homogeneous hemodynamic processes over the brain; several studies have pointed out that this is indeed not the case and that we are faced with variable HRF latency across physiological processes and distinct brain regions (Roebroek et al., 2011; Valdes-Sosa et al., 2011). Recently, a number of studies have addressed this issue proposing to model the HRF according to several recipes (Bakhtiari and Hossein-Zadeh, 2012; Havlicek et al., 2011, 2010; Ryali et al., 2011). As well, a recent study has proposed that it would still be feasible to infer connectivity at BOLD level, under the assumption that Granger causality is theoretically invariant under filtering (Barnett and Seth, 2011) and that the HRF can be considered as a filter. It is still unclear whether and how specific effects related to HRF disturb the inference of temporal precedence. In addition a simulated or experimental ground truth is difficult to obtain, though some studies on simulated fMRI data have tried to reveal the relationship between neural-level and BOLD-level causal influence (Deshpande et al., 2010; Smith et al., 2011). A considerable help to obtain the HRF for deconvolution could come from multimodal imaging where the high temporal resolution of EEG is combined to the high spatial resolution of fMRI, but this experimental approach is still far from being optimal and widely applicable. HRF has been studied almost since the early days of fMRI (Handwerker et al., 2012). For task-related fMRI, neural population dynamics can be captured by modeling signal dynamics with explicit exogenous inputs (Friston et al., 2008; Riera et al., 2004), i.e. deconvolution according to the explicit task design is possible in this case (Buxton et al., 1998; Friston et al., 2000; Glover, 1999). For resting-state fMRI on the other hand, the absence of explicit inputs makes this task more difficult, unless relying on some specific prior physiological hypothesis (Friston et al., 2008; Havlicek et al., 2011). In order to overcome these issues and to allow a more general approach, here we present a simple and novel blind-deconvolution technique for BOLD-fMRI signal.

Coming to the second limitation, in order to distinguish among direct

and mediated influences in multivariate datasets it is necessary to condition the analysis to other variables. A bivariate analysis would indeed lead to the detection of many false positives. In presence of a large number of variable and short time series, a fully multivariate conditioning could lead to computational problems due to the overfitting. Furthermore, conceptual issues would arise in presence of redundant variables (Angelini et al., 2010; Marinazzo et al., 2010). In this paper we thus apply partial conditioning for Granger Causality (PCGC)¹ to a limited subset of variables, as recently proposed (Marinazzo et al., 2012) for reconstructing the BOLD and deconvolved BOLD level effective connectivity network (ECN) and compare them.

2. Materials and methods

2.1. Blind-deconvolution in resting-state fMRI data

Hemodynamic deconvolution of BOLD signal is performed as described in (David et al., 2008; Glover, 1999). Under the assumption that the transformation from neural activation to BOLD response can be modeled as a linear and time invariant system, measured fMRI data $b(t)$ can be seen as the result of the convolution of neural states $s(t)$ with a HRF $h(t)$:

$$b(t) = s(t) \otimes h(t) + \epsilon(t) \quad (1)$$

Where t is the time and \otimes denotes convolution. $\epsilon(t)$ is the noise in the measurement, which we assume to be white. Since the right side of the above equation includes three unobservable quantities, in order to solve the equation for $h(t)$ we need to substitute $s(t)$ with a hypothetical model of the neural activation for $s(t)$. Here we employ a simple on-off model of activation to model $s(t)$:

$$\hat{s}(t) = \sum_{\tau=0}^{\infty} \delta(t - \tau) \quad (2)$$

where $\delta(t - \tau)$ is the delta function. This allows to fit the HRF $h(t)$ according to $\hat{s}(t)$ using a canonical HRF (two gamma functions) and two derivatives (multivariate Taylor expansion: temporal derivative and dispersion derivative) (Friston et al., 2000), as is common in most fMRI studies.

¹Please note that this approach is different from partial Granger causality (PGC) (Guo et al. (2008), Journal of Neuroscience Methods, **172**, 79)

Once calculated $h(t)$, we can obtain an approximation $\tilde{s}(t)$ of the neural signal from the observed data using a Wiener filter

$$\tilde{s}(t) = d(t) \otimes b(t) \quad (3)$$

Let $H(\omega)$, $B(\omega)$, $E(\omega)$, and $D(\omega)$ be the Fourier transforms of $h(t)$, $b(t)$, $\epsilon(t)$, and $d(t)$, respectively. Then

$$D(\omega) = \frac{H^*(\omega)}{|H(\omega)|^2 + |E(\omega)|^2}, \quad (4)$$

where $*$ denotes complex conjugate. The estimation $\tilde{s}(t)$ of the neural states $s(t)$ is then given by

$$\tilde{s}(t) = FT^{-1} \{D(\omega)B(\omega)\} = FT^{-1} \left\{ \frac{H^*(\omega)B(\omega)}{|H(\omega)|^2 + |E(\omega)|^2} \right\}. \quad (5)$$

Where FT^{-1} is the inverse Fourier transform operator.

For task-related fMRI, the stimulus function provides the prior expectations about neural activity and a generative model whose inversion corresponds to deconvolution; this is in principle not the case for resting-state fMRI. Nonetheless there is increasing evidence of specific events and neural states that govern the dynamics of the brain at rest (Deco and Jirsa, 2012; Petridou et al., 2012). Furthermore, Tagliazucchi et al. proposed that these events are reflected by relatively large amplitude BOLD signal peaks and thus that such fluctuations could encode relevant information from resting-state fMRI recordings (Tagliazucchi et al., 2012). Inspired by their work, we consider resting-state fMRI as *spontaneous event-related*, and we propose to extract the HRF from those pseudo-events. After doing this, we can employ the deconvolution model in the same way as described above. It is known that the BOLD response is much slower than the neural activation that is presumed to drive it. Consequently, the peak of the BOLD signal lags behind the peak of neural activation (i.e. by κ points). So here we assume that these events are generated from $\hat{s}(t)$.

Glover pointed out that the noise spectrum in task-related fMRI can be obtained from time series measurements in nonactivated cortical regions (Glover, 1999); here we extend the model to cope with resting-state fMRI for

which there is no explicit activation. In this study we assumed covariance of noise ϵ equal to $cov [b(t) - \hat{s}(t) \otimes h(t)]$.

In order to obtain a value for κ , we search all integer values in the interval $[0 \ \kappa_{max}]$, where κ_{max} is an arbitrary maximum value, choosing the one for which the noise error covariance is smallest as the onset. By this method we can perform deconvolution on all BOLD signals, requiring no information on timing or a priori spatial information of events; furthermore, the time series could be the average of time series over a region of interest with any scale, or series extracted by independent or principal component analysis. A flow chart for BOLD signal deconvolution is shown in Fig.1.

This is the pseudo-code for our procedure.

Pseudo-code

- i Preprocess time series (e.g. detrend, normalize etc.).
- ii Find a time set S in which the BOLD values exceed a given threshold around a local maximum.
- iii choose a maximum time delay κ_{max}
FOR $n = 0$ to κ_{max}

$$S_n = S - n$$

$$\hat{s}_n(t) = 1, t \in S_n; \hat{s}_n(t) = 0, t \notin S_n.$$

Fit a general linear model using \hat{s}_n and canonical HRF with time and dispersion derivatives.

END FOR

- iv Let $\epsilon_\kappa = \min_{0 \leq n \leq \kappa_{max}} \{\epsilon_n\}$, where $\epsilon_n = cov [b(t) - \hat{s}_n(t) \otimes h_n(t)]$.

- v Follow equation 4 and 5, using HRF h_κ and ϵ_κ for deconvolution, get $\tilde{s}(t)$.

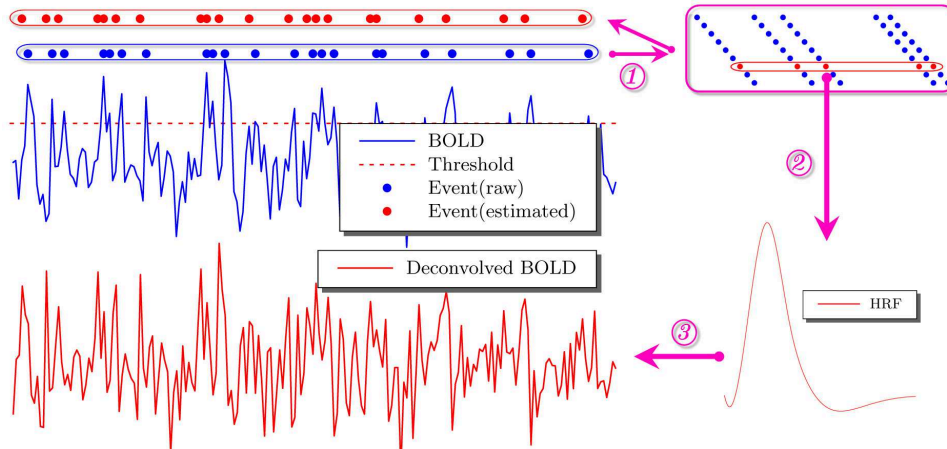


Figure 1: Flow chart for blind-deconvolution procedure. 1. the pre-processed (detrended and normalized) observed BOLD signal is evaluated against a given threshold obtaining several sets of putative onsets for pseudo-events. 2. the time deviation of the timing sets is adjusted; the set with smallest noise error covariance will represent the event. 3. the observed BOLD signal is deconvolved into a neural signal by using the corresponding HRF.

2.2. Partially conditioned Granger causality

Here we employ a methodology proposed in (Marinazzo et al., 2012) which allows to compute Granger causality conditioned to a limited number of variables in the framework of information theory. The idea is that conditioning on a small number of variables, chosen as the most informative for the candidate driver variable, is sufficient to remove indirect interactions for sparse connectivity patterns.

We consider n covariance-stationary variables $\{x_i(t)\}_{i=1,\dots,n}$, denoting the state vectors as:

$$X_\alpha(t) = (x_\alpha(t-m), \dots, x_\alpha(t-1)) \quad (6)$$

m being the model order. Let $\epsilon(x_\alpha|Y)$ be the mean squared error prediction of x_α on the basis of the vectors Y . The partially conditioned Granger causality index $c(\beta \rightarrow \alpha)$ is defined as follows:

$$c(\beta \rightarrow \alpha) = \log \frac{\epsilon(x_\alpha|\mathbf{Z})}{\epsilon(x_\alpha|\mathbf{Z} \cup X_\beta)} \quad (7)$$

Where $\mathbf{Z} = \{X_{i_1}, \dots, X_{i_{n_d}}\}$ is a set of the n_d variables, in $\{X_1, X_2, \dots, X_n\} \setminus X_\beta$, which are most informative for X_β . We adopt the following approximate strategy for \mathbf{Z} : given the previous Z_{k-1} , the set Z_k is obtained adding the variable with greatest information gain. This is repeated until n_d variables are selected.

2.3. Simulation Datasets: NetSim

A method for establishing a ground truth for fMRI data has not reached a general consensus. Recently a benchmark dataset, NetSim (Smith et al., 2011) has attracted a lot of attention. Previous studies have shown that lag-based methods perform very poorly on these datasets; it is anyway worthy to mention that these data are simulated under the DCM framework, contain no reciprocal connections and only Gaussian noise, limiting their universality as ground truth. Here we analyzed the largest of these datasets, consisting of 50 nodes. After deconvolution the sensitivity improved significantly, increasing from 20% to 30%. Also the specificity improved from 88% to 94%. This does not render GC the method of choice for these data, for which we also have to point out that "neural events" and noise are not distinguishable, but gives nonetheless an indicative result for the usefulness of deconvolution of the BOLD signal.

2.4. Resting-State fMRI Datasets

In order to investigate the role of repetition time (TR) on the deconvolution procedure and on the effective network reconstruction, our analyses were performed on a resting-state fMRI dataset which has been publicly released in the "1000 Functional Connectomes Project"². All participants had no history of neurological and psychiatric disorders and all gave the informed consent approved by local Institutional Review Board. During the scanning participants were instructed to keep their eyes closed, not to think of anything in particular, and to avoid falling asleep.

Two data sets with different TR (TR=1.4s and TR=0.645s) were acquired on Siemens 3T Trio Tim scanners using developed multiplexed echo planar

²http://fcon_1000.projects.nitrc.org, accessed march 2012.

imaging (Feinberg et al., 2010). As specified in detail below, two resting-state fMRI data are included in the protocol - a TR=0.645s (3mm isotropic voxels, 10 minutes) to provide optimal temporal resolution and TR=1.4s (2mm isotropic voxels, 10 minutes) to provide optimal spatial resolution. The third data set, acquired on a 4T scanner, contains standard resting-state fMRI acquisitions with a longer TR (TR=3, 4mm isotropic voxels, 5 minutes). For more detail on subject and data information, please see website^{2, 3}.

2.5. Data preprocessing

Preprocessing of resting-state images was performed using the Statistical Parametric Mapping software (SPM8, <http://www.fil.ion.ucl.ac.uk/spm>). The preprocessing included slice-timing correction relative to middle axial slice for the temporal difference in acquisition among different slices, head motion correction, spatial normalization into the Montreal Neurological Institute stereotaxic space, resampling to 3-mm isotropic voxels. 8(9) subjects were excluded from the dataset with TR=0.645s (TR=1.4s) because either translation or rotation exceeded ± 1.5 mm or $\pm 1.5^\circ$, resulting in 16(TR=0.645s) and 15(TR=1.4s) subjects each one scanned in two sessions which were used in the analysis). One subject whose data were too noisy was excluded from the TR=3 dataset, resulting in 10 subjects used in the analysis. In order to avoid introducing artificial local spatial correlations between voxels, no spatial smoothing was applied for further analysis, as previously suggested (Zhang et al., 2011; Salvador et al., 2005; Liao et al., 2011).

2.6. Anatomical parcellation and analysis

The functional images were segmented into 90 regions of interest (ROI) using automated anatomical labeling (AAL) template as reported in previous studies. For each subject, the representative time series of each ROI was obtained by averaging the fMRI time series across all voxels in the ROI (Salvador et al., 2005). Several procedures were used to remove possible spurious variances from the data through linear regression. These were i) six head motion parameters obtained in the realigning step, ii) signal from a region in cerebrospinal fluid, iii) signal from a region centered in the white matter, iv) global signal averaged over the whole brain. The BOLD time

³http://fcon_1000.projects.nitrc.org/indi/pro/eNKILRS.TRT/FrontPage.html.

series were deconvolved into neural state signal using the above mentioned approach.

2.7. Effective connectivity network analysis

The topological properties of the effective connectivity network were defined on the basis of a 90×90 binary directed graph G , consisting of nodes and directed edges:

$$e_{ij} = \begin{cases} 1, & F_{i \rightarrow j} > T; \\ 0, & \text{otherwise} \end{cases} \quad (8)$$

Where e_{ij} refers to the directed edge from ROI i to ROI j in the graph. T indicates the threshold. In a directed graph e_{ij} is not necessarily equal to e_{ji} . Considering that the graph we focused on is directed, all topological properties were calculated on incoming and outgoing matrix, respectively. Graph theoretical analyses were carried out on the effective connectivity network using the Brain Connectivity Toolbox (Rubinov and Sporns, 2010).

2.8. Threshold selection

As previous studies suggested that the brain networks of each subject normally differ in both the number and weighting of the edges (Zhang et al., 2011; Liao et al., 2011), we applied a matching strategy to characterize the properties of effective connectivity network. Both the global and local network efficiencies have a propensity for being higher with greater numbers of edges in the graph (Wen et al., 2011). Modifying the sparsity values (number of edges) of the adjacency matrix also altered the graph's structure. As a consequence it was suggested that the graphs to be compared must have (a) the same number of nodes and (b) the same number of edges (Bullmore and Bassett, 2011). The cost was defined as the ratio of the number of existing edges divided by the maximum possible number of edges in a network. Since there is currently no formal consensus regarding selection of cost thresholds, here we selected a range of 0.05 to 0.14 with step = 0.01 for subsequent network analyses. The lower bound was chosen as the one yielding a sparse graph with mean degree $\geq 2\ln(90)$ (total number of edges ≥ 405 where $405/90^2 = 0.05$). The upper threshold corresponded to the smallest significant value of Granger causality (F-test with $p = 0.05$) across all subjects).

2.9. Network metrics

For effective connectivity network at each cost threshold, we calculated both overall topological properties and nodal characteristics (Rubinov and Sporns, 2010). The overall topological properties included i) small-worldness (σ), related to normalized clustering coefficient (γ) and normalized characteristic path length (λ); ii) network efficiency, divided in local efficiency (E_{loc}) and global efficiency (E_{glob}). The nodal characteristics included i) the nodal degree, that quantifies the extent to which a node is relevant to the graph, and ii) the nodal efficiency, that quantifies the importance of the nodes for the communication within the network (Bassett and Bullmore, 2006). Furthermore we calculated the area under the curve (AUC) across all cost values for the above mentioned network properties. This quantity represents a summarized scalar for topological characterization of brain networks independent of single cost threshold selection.

3. Results

3.1. Reconstruction of HRF

We tested the proposed deconvolution method on resting-state fMRI data; following the procedure summarized in the box, firstly we set a maximum time lag from a given threshold crossing, and obtain an optimal value for this lag, denoted with κ . The histograms for κ , reported in Fig.2 show a maximum around $4 \sim 6$ s, which is consistent with a previous study according to which the latency delay is $4 \sim 8$ s in gray matter (Lee et al., 1995). It is worth to mention that the lower TR could allow a more accurate estimation of the lag.

To assess the effect of deconvolution, we compared the shape of voxel based HRF over the whole brain using different TRs. We focused on three parameters: response height, time-to-peak, and full-width at half-max (FWHM) as potential measures of response magnitude, latency, and duration. Using principal component analysis we determined the average intersubject variability of HRF maps. We found that the first component of HRF accounted for $81.7 \pm 2.9\%$ (response height), $98.1 \pm 1.2\%$ (time to peak) and $95.6 \pm 3.5\%$ (FWHM) of the variance. Furthermore, the spatial distribution is very similar to the mean group map. The mean group results are plotted in Fig.3. The response height, time to peak and FWHM of HRFs differ across brain regions, as a consequence of multiple factors including neural activity differences, global magnetic susceptibilities, vascular differences, baseline

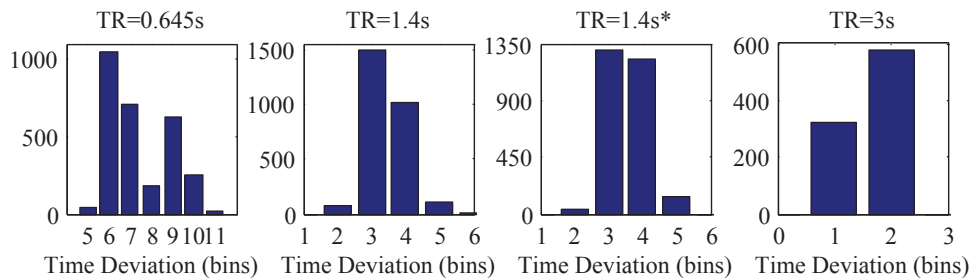


Figure 2: Histogram of the values of time deviation κ . (*:without regression of global signal)

cerebral blood flow, slice timing differences etc. (Handwerker et al., 2004). These patterns are remarkably similar across subjects and TRs, reflecting the robustness of the proposed approach.

3.2. Variance stability of causality matrix

As another indicator of the stability of the proposed joint of deconvolution and PCGC approach we tested the variance of causality matrix across all subjects. We calculated the variance of the Granger causality matrix obtained both on the BOLD and deconvolved BOLD level signal. Firstly, we converted the matrix to Z-scores, then we calculated the variance of each matrix element, finally summing up the all these values into an overall variance index. The variance of Granger causality matrix obtained from the deconvolved signal is much lower than the one of the BOLD level matrix for all TR values (Fig.4). Also, PCGC method kept the variance lower than full conditioned GC method. This result was confirmed testing a network at another scale using 1024 nodes (Fig.4, the native AAL segmentation was parcellated into 1024 micro regions of interest of approximately identical size across both hemispheres (Zhang et al., 2011); in this case we could not test full conditioned GC due to small number of samples).

3.3. Global signal regression

As shown in previous studies, several sources of spurious variance should be removed by regression: motion artifacts, white matter and ventricular time courses. Still, the effects of regression against the global signal, calculated by averaging across all voxels within a whole brain mask, are debated.

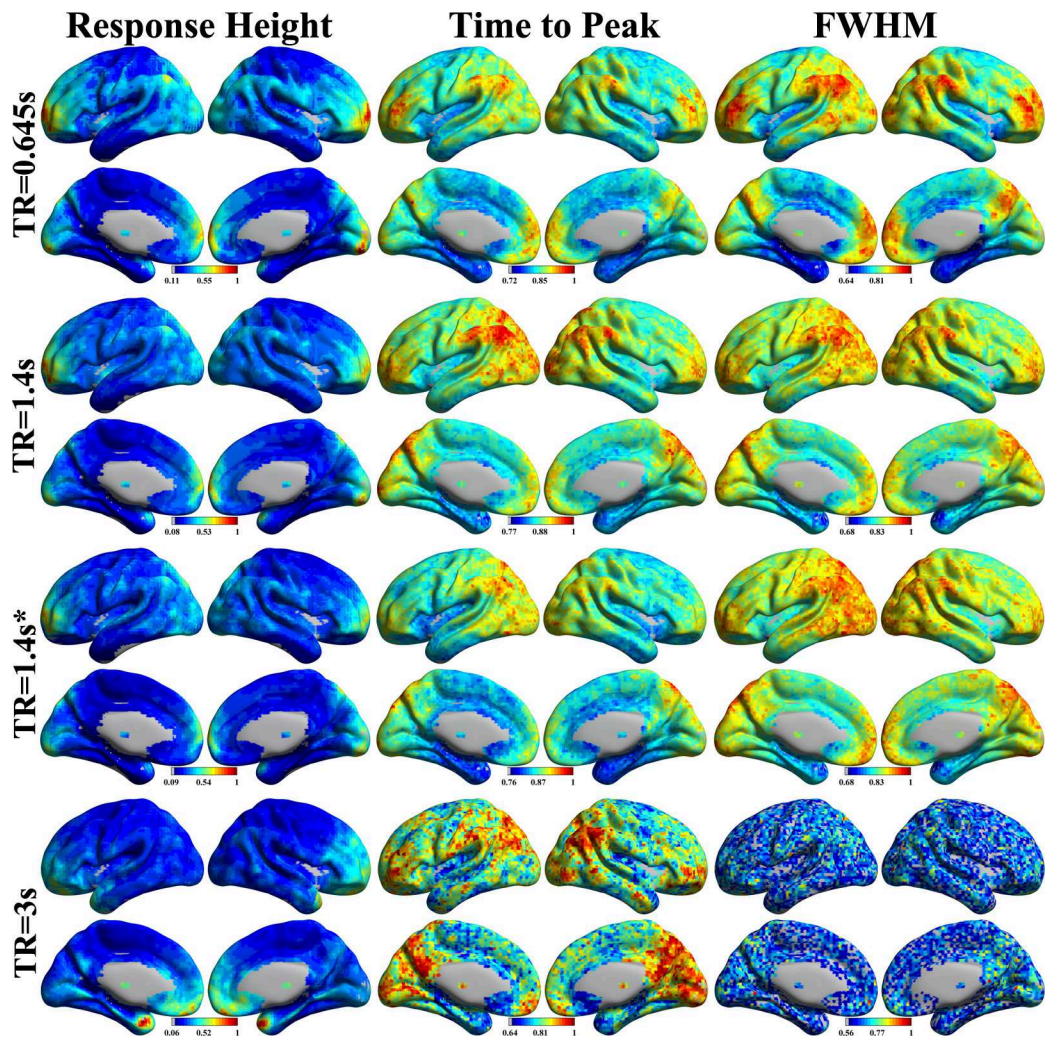


Figure 3: Spatial distribution of HRF shape: response height, time to peak and full-width at half-max (all values have been normalized, keeping range from 0 to 1).(*:without regression of global signal)

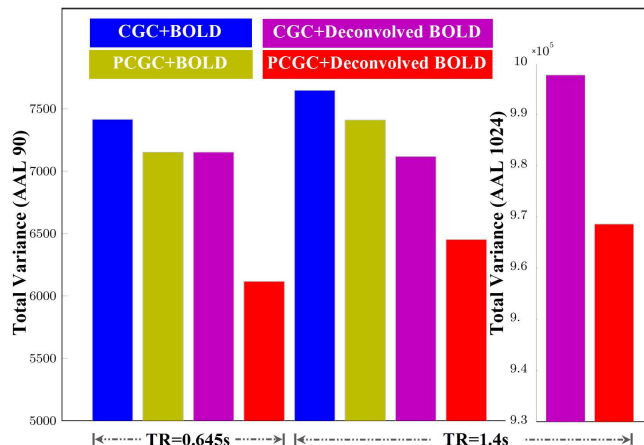


Figure 4: Total variance of causality matrix across all subjects. Full conditional Granger causality (CGC) and PCGC combined with BOLD and deconvolved BOLD level signal were used for construction of causality matrix.

In order to evaluate this effect on our data we calculated spatial correlation between the the group mean image of HRF(response height, time to peak, FWHM) with and without regression of global signal in the preprocessing step, obtaining high Pearson correlation between them: $r=0.97$ (response height), 0.90 (time to peak), 0.88 (FWHM). We can thus conclude that regression against global signal still preserved the spatial distribution.

3.4. Effective connectivity network recovery with partial conditioning

When trying to reconstruct effective connectivity networks, we are faced with the problem of coping with a large number of variables, when the application of multivariate Granger causality may be questionable or even unfeasible, whilst bivariate Granger causality would detect also indirect interactions. Conditioning on a large number of variables requires an high number of samples in order to get reliable results. Reducing the number of variables that one has to condition over would thus provide better results for small data-sets. In the general formulation of Granger causality, one has no way to choose this reduced set of variables; on the other hand, in the framework of information theory, it is possible to individuate the most informative variables one by one.

The optimal model order m (order of the autoregressive model in Granger causality, embedding dimension in transfer entropy) for deconvolved BOLD

and BOLD signal was determined by leave-one-out cross-validation, and was found to be 3 for TR=0.645s, 2 for TR=1.4s and 1 for TR=3s. Under the Gaussian assumption, we constructed effective connectivity network using PCGC method. We firstly have to determine the number of variables upon which conditioning. To do this we look at how much uncertainty we eliminate adding an extra variable, letting the number of conditioning variables included n_d vary from 1 to 20. This uncertainty can be expressed in terms of the information that we gain adding an extra variable. In Fig.5, we plot the information gain as a function of n_d ; as expected, both this quantity and its increment decrease monotonically with n_d .

We can observe that the knee of the curves occurs when six variables are considered. This happens also when we consider different brain prior templates with 17 or 160 nodes (results not reported here). This could be connected to the fact that the average number of modules which explain the equal-time correlations of resting brain is close to six (Marinazzo et al., 2010; Salvador et al., 2005), therefore picking one variable from each module is sufficient to have most of the information, about a given channel, that can be obtained from the remaining channels, and this independently on the number of nodes. The effect of deconvolution, for the information gain, is to qualitatively raise the curve for TR=0.645s, and to lower them for TR=1.4s. This trend (not statistically significant) might be the result of two competing effects, the fact the deconvolution may remove spurious correlations and/or restore genuine correlations obscured by noise.

Synthesizing the knee of the curves, sensitivity and specificity, we consider $n_d = 10$ as the most appropriate number of most informative variables to include in the conditioning procedure.

3.5. Global characteristics of ECN

The global topological properties of brain ECN at deconvolved BOLD and BOLD level rely on the choice of thresholds. We used multiple cost thresholds and the AUC to evaluate the stability of the topological organization (Table 1). An higher number of differences between the two networks was found with a (relatively) longer TR (TR=1.4s). Specifically, the AUC of small-worldness (σ), normalized clustering coefficient (γ), clustering coefficient (C_p) and local efficiency (E_{loc}) displayed the most significant differences, similar to

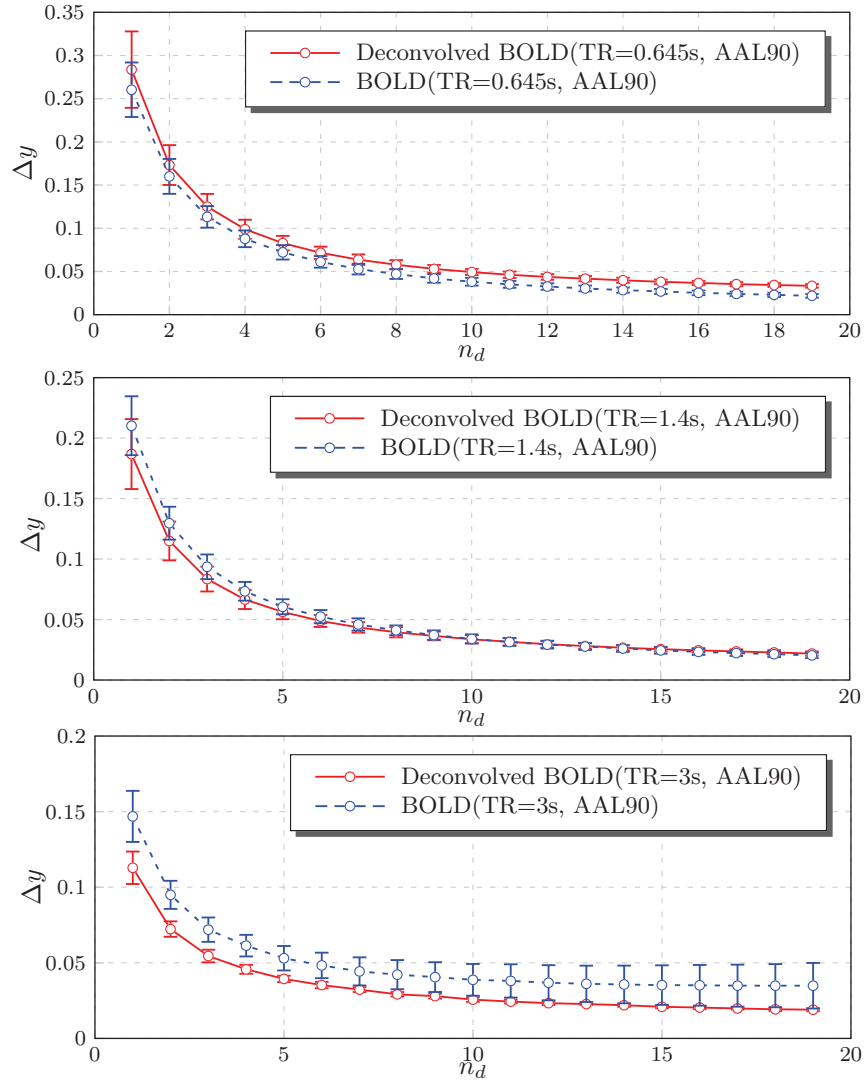


Figure 5: The mutual information gain (Δy), when the $(n_d + 1)$ -th variable is included, is plotted versus n_d . The information gain is averaged over all the variables.

Global network parameter	AUC difference			
	TR=0.645s		TR=1.4s	
	Incoming	Outgoing	Incoming	Outgoing
Sigma(σ)	Y	N	Y	Y
Lambda(λ)	N	N	N	N
Gamma(γ)	Y	N	Y	Y
Characteristic path length(L_p)	N	Y	Y	N
Clustering coefficient(C_p)	Y	N	Y	Y
Global efficiency(E_{glob})	N	Y	Y	N
Local efficiency(E_{loc})	Y	N	Y	Y

Table 1: Comparison of AUC between deconvolved BOLD and BOLD. $n_d = 10$, Y: $p < 0.05$, FDR corrected; N: otherwise.

what emerged with TR=0.645s. For the data set with shorter TR we found significant differences in the characteristic path length and global efficiency of the outgoing network, whereas the most relevant differences were found for the incoming network with the longer TR.

3.6. Nodal characteristics of ECN

Comparing the two networks on nodal degree, nodal global efficiency and nodal local efficiency revealed modifications in deconvolved BOLD and BOLD level (Fig.6). The patterns of nodal degree modifications resembled to those of nodal global efficiency in incoming network in both TR=0.645s and TR=1.4s fMRI data sets. In addition, more brain regions showed modified nodal degree and (global/local) efficiency in TR=0.645s rather than TR=1.4s data.

4. Discussion

In this study we proposed a novel methodology to achieve deconvolution in resting state data using spontaneous pseudo events, and to apply partially conditioned Granger Causality to the analysis of fMRI data. In our opinion this joint approach is the most convenient to infer effective connectivity with Granger Causality from resting state fMRI data.

In the absence of a well defined ground truth, and in the light of the still active and unresolved debate on the usefulness of HRF deconvolution

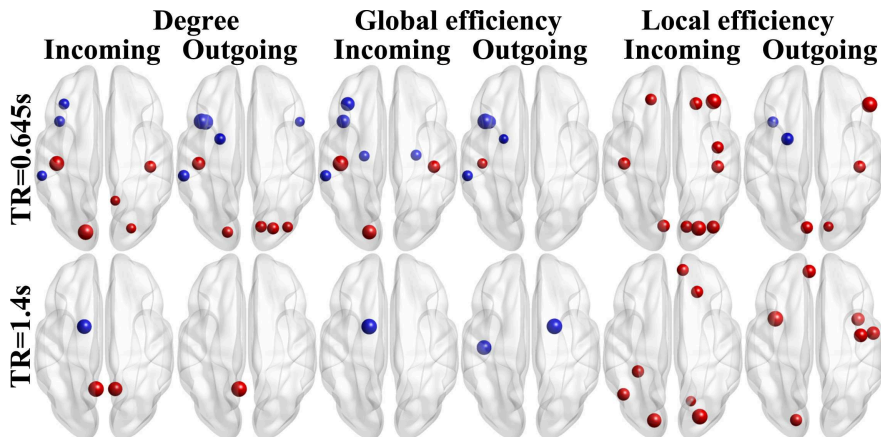


Figure 6: Z-scores for Area under Curve from regional nodal parameters (deconvolved BOLD vs BOLD), $p < 0.05$, FDR corrected, ($n_d = 10$). Blue indicate negative values, red positive values. The point size is proportional to the absolute Z value.

Granger causality based connectivity, we limit ourselves to validate the stability of the proposed method and indicate a possible path for the continuation of this debate, quantifying and comparing the overall topological properties of large-scale ECNs on deconvolved BOLD-level versus BOLD-level signals, investigating also the effect of different time resolutions (TR=0.645s and TR=1.4s).

Previous discussions on evaluating effective connectivity from fMRI data reached the conclusion that it is better to use state-space model for inferring causality on hidden neural states (Valdes-Sosa et al., 2011; Ryali et al., 2011; Bakhtiari and Hossein-Zadeh, 2012). A pioneering EEG-fMRI study provided the first experimental substantiation of the theoretical possibility to improve interregional coupling estimation from hidden neural states of fMRI (David et al., 2008). Though promising (Friston, 2009), these implications are still limited by the fact that multimodal recording is invasive and not applicable to healthy controls. As a consequence, data-driven methods for substantiating the confounding variability of haemodynamics have been developed. The two available types of state space models in estimation of HRF (Valdes-Sosa et al., 2011): the generic (linear canonical/spline HRF) (Glover, 1999; Marrelec et al., 2003) and biophysically informed models (DCM non-linear HRF)(Friston et al., 2000). Generic models are widely applicable but

lack specific biophysical constraints (Glover, 1999; Marrelec et al., 2003), while biophysically informed models are constrained by the hypothesis itself (Friston et al., 2000). A recently proposed, biophysically informed blind deconvolution approach based on the state-of-the-art Cubature Kalman filtering could be a useful tool for resting-state fMRI (Havlicek et al., 2011). In the present study, however, we use a simpler approach which employs the generic linear canonical HRF for deconvolution. It is worth to point out that the significant differences between BOLD- and deconvolved BOLD-level effective connectivity found in complex network measures cannot absolutely exclude the misestimation of HRF. Furthermore HRF latency effect does not always critically affect the evaluation of mutual influence, so ECNs on BOLD and deconvolved BOLD level could have important consistencies (Supekar and Menon, 2012).

Findings from brain connectivity studies have now demonstrated that the human brain network exhibits robust small-world topological properties, not only in the anatomical connectivity (reconstructed by diffusion tractography) (Hagmann et al., 2008) and functional connectivity network (Salvador et al., 2005), but also in effective connectivity network (Liao et al., 2011). The current results also suggested that the ECNs obtained from BOLD and deconvolved data, with shorter and longer TR, have prominent small-world attributes, which would thus be confirmed as a general signature of robust organization of complex brain networks. Small-worldness indicates indeed an optimal balance between segregated and integrated organization to process the information (Bassett and Bullmore, 2006). For relatively longer TR we found significant differences between BOLD and deconvolved ECNs. Although an explanation based on precise neurobiological mechanisms is still not evident, we can suggest that the BOLD effect results from a more complex sequence of effects linking neuronal activity, vascular changes and MRI signal (Logothetis, 2008). Hemodynamic delay, and hence the correct onset of the events is indeed hard to capture with a long TR (Laufs et al., 2008).

In complex networks organization, the normalized clustering coefficient and the clustering coefficient are two key measures. They quantify the extent of local cliquishness or of local efficiency of information transfer of a network (Bullmore and Bassett, 2011), reflecting the local properties of network topologies. For longer TR, we observed significant differences between the two level ECNs. Thus the short-scale or local-scale network proper-

ties are indeed affected by deconvolution. Moreover, the normalized characteristic path length and the characteristic path length quantify global efficiency or the capability for parallel information propagation of a network (Bullmore and Sporns, 2009). These two measurements along with global efficiency are mainly associated with long-range connections ensuring effective interactions or rapid transfers of information (He et al., 2009). It is widely accepted that long-range axonal connectivity being an important indicator of the functional-anatomical organization of the human cortex (Knösche and Tittgemeyer, 2011). This study reported no differences in long-range network organization.

It is known that resting-state functional connectivity studies using either seed functional connectivity or independent component analysis benefit from higher sampling rates to adequately sample undesirable respiration and cardiac effects (Birn et al., 2008), while for event-related fMRI, faster sampling could allow for a better characterization of the hemodynamic response. The same applies to GCA. The previous simulations showed that accuracy of Granger causality depends on volume TR, faster sampling interval increased the detection capacity of GCA of fMRI data to neural causality (Deshpande et al., 2010; Roebroek et al., 2005). In this paper, we focus on resting-state fMRI data with TR=0.645s and 1.4s to maximally escape information loss due to low sampling. Considering the limitation of acquisition sequence, the conventional fast TR data acquisition brings to the loss of the fine spatial resolution (Huettel et al., 2004; Kim et al., 1994).

Other methodological considerations are worth to be mentioned. The first one concerns data preprocessing. As a general idea spatial smoothing can reduce the noise and increase signal-to-noise ratio, therefore improving the accuracy of detecting of neural event (Huettel et al., 2004). Here we do not include this step. As we used AAL template, spatial smoothing would blur the boundary among these regions, which may affect the GC inference. Temporal filtering is frequently a necessary step for functional connectivity analysis of resting-state fMRI data. In line with previous studies that considered a low model order in GCA (Hamilton et al., 2010; Liao et al., 2011), we did not performed low-pass filtering.

Secondly, graph theoretic approach is one of the most powerful and flexible approaches to investigate functional and structural brain connectome;

still some controversies remain, concerning the definition of network nodes and edges (Bullmore and Bassett, 2011; Wig et al., 2011). Different node definitions by prior anatomic brain templates (Wang et al., 2009) or node scales (Fornito et al., 2010; Zalesky et al., 2010) could produce different results. In future works, more brain templates and more node scales comparison for effective connectivity network should be explored.

Acknowledgments

H. Chen was supported by the Natural Science Foundation of China (No. 61125304 and No. 61035006). G.R. Wu gratefully acknowledges the financial support from China Scholarship Council(2011607033).

References

References

- Angelini, L., De Tommaso, M., Marinazzo, D., Nitti, L., Pellicoro, M., Stramaglia, S., 2010. Redundant variables and Granger causality. *Physical Review E* 81, 037201.
- Bakhtiari, S., Hossein-Zadeh, G., 2012. Subspace-based identification algorithm for characterizing causal networks in resting brain. *NeuroImage* 60, 1236 – 1249.
- Barnett, L., Barrett, A., Seth, A., 2009. Granger causality and transfer entropy are equivalent for gaussian variables. *Physical Review Letters* 103, 238701.
- Barnett, L., Seth, A.K., 2011. Behaviour of Granger causality under filtering: theoretical invariance and practical application. *Journal of Neuroscience Methods* 201, 404 – 419.
- Bassett, D., Bullmore, E., 2006. Small-world brain networks. *The neuroscientist* 12, 512–523.
- Birn, R., Murphy, K., Bandettini, P., 2008. The effect of respiration variations on independent component analysis results of resting state functional connectivity. *Human brain mapping* 29, 740–750.

- Bressler, S., Seth, A., 2011. Wiener-Granger causality: A well established methodology. *Neuroimage* 58, 323–329.
- Büchel, C., Friston, K., 1997. Modulation of connectivity in visual pathways by attention: cortical interactions evaluated with structural equation modelling and fMRI. *Cerebral Cortex* 7, 768–778.
- Bullmore, E., Bassett, D., 2011. Brain graphs: graphical models of the human brain connectome. *Annual Review of Clinical Psychology* 7, 113–140.
- Bullmore, E., Sporns, O., 2009. Complex brain networks: graph theoretical analysis of structural and functional systems. *Nature Reviews Neuroscience* 10, 186–198.
- Buxton, R., Wong, E., Frank, L., 1998. Dynamics of blood flow and oxygenation changes during brain activation: the balloon model. *Magnetic Resonance in Medicine* 39, 855–864.
- David, O., Guillemain, I., Sallet, S., Reyt, S., Deransart, C., Segebarth, C., Depaulis, A., 2008. Identifying neural drivers with functional MRI: an electrophysiological validation. *PLoS Biology* 6, e315.
- Deco, G., Jirsa, V., 2012. Ongoing cortical activity at rest: criticality, multistability, and ghost attractors. *The Journal of Neuroscience* 32, 3366–3375.
- Deshpande, G., Sathian, K., Hu, X., 2010. Effect of hemodynamic variability on Granger causality analysis of fMRI. *Neuroimage* 52, 884–896.
- Feinberg, D., Moeller, S., Smith, S., Auerbach, E., Ramanna, S., Glasser, M., Miller, K., Ugurbil, K., Yacoub, E., 2010. Multiplexed echo planar imaging for sub-second whole brain fMRI and fast diffusion imaging. *PLoS One* 5, e15710.
- Fornito, A., Zalesky, A., Bullmore, E., 2010. Network scaling effects in graph analytic studies of human resting-state fMRI data. *Frontiers in Systems Neuroscience* 4.
- Friston, K., 2009. Causal modelling and brain connectivity in functional magnetic resonance imaging. *PLoS Biology* 7, e1000033.
- Friston, K., Harrison, L., Penny, W., 2003. Dynamic causal modelling. *Neuroimage* 19, 1273–1302.

- Friston, K., Mechelli, A., Turner, R., Price, C., 2000. Nonlinear responses in fMRI: the balloon model, volterra kernels, and other hemodynamics. *NeuroImage* 12, 466–477.
- Friston, K., Trujillo-Barreto, N., Daunizeau, J., 2008. Dem: a variational treatment of dynamic systems. *Neuroimage* 41, 849–885.
- Glover, G., 1999. Deconvolution of impulse response in event-related bold fMRI. *NeuroImage* 9, 416–429.
- Hagmann, P., Cammoun, L., Gigandet, X., Meuli, R., Honey, C., Wedeen, V., Sporns, O., 2008. Mapping the structural core of human cerebral cortex. *PLoS Biology* 6, e159.
- Hamilton, J., Chen, G., Thomason, M., Schwartz, M., Gotlib, I., 2010. Investigating neural primacy in major depressive disorder: multivariate Granger causality analysis of resting-state fMRI time-series data. *Molecular Psychiatry* 16, 763–772.
- Handwerker, D., Gonzalez-Castillo, J., D’Esposito, M., Bandettini, P., 2012. The continuing challenge of understanding and modeling hemodynamic variation in fMRI. *NeuroImage* 62, 1017–1023.
- Handwerker, D., Ollinger, J., D’Esposito, M., 2004. Variation of bold hemodynamic responses across subjects and brain regions and their effects on statistical analyses. *Neuroimage* 21, 1639–1651.
- Havlicek, M., Friston, K., Jan, J., Brazdil, M., Calhoun, V., 2011. Dynamic modeling of neuronal responses in fMRI using cubature Kalman filtering. *NeuroImage* 56, 2109 – 2128.
- Havlicek, M., Jan, J., Brazdil, M., Calhoun, V., 2010. Dynamic Granger causality based on Kalman filter for evaluation of functional network connectivity in fMRI data. *NeuroImage* 53, 65–77.
- He, Y., Dagher, A., Chen, Z., Charil, A., Zijdenbos, A., Worsley, K., Evans, A., 2009. Impaired small-world efficiency in structural cortical networks in multiple sclerosis associated with white matter lesion load. *Brain* 132, 3366–3379.

- Huettel, S., Song, A., McCarthy, G., 2004. Functional magnetic resonance imaging. volume 1. Sinauer Associates Sunderland, MA.
- Kim, S., Hendrich, K., Hu, X., Merkle, H., Ugurbil, K., 1994. Potential pitfalls of functional MRI using conventional gradient-recalled echo techniques. *NMR in Biomedicine* 7, 69–74.
- Knösche, T., Tittgemeyer, M., 2011. The role of long-range connectivity for the characterization of the functional–anatomical organization of the cortex. *Frontiers in systems neuroscience* 5.
- Laufs, H., Daunizeau, J., Carmichael, D., Kleinschmidt, A., 2008. Recent advances in recording electrophysiological data simultaneously with magnetic resonance imaging. *Neuroimage* 40, 515–528.
- Lee, A., Glover, G., Meyer, C., 1995. Discrimination of large venous vessels in time-course spiral blood-oxygen-level-dependent magnetic-resonance functional neuroimaging. *Magnetic Resonance in Medicine* 33, 745–754.
- Liao, W., Ding, J., Marinazzo, D., Xu, Q., Wang, Z., Yuan, C., Zhang, Z., Lu, G., Chen, H., 2011. Small-world directed networks in the human brain: multivariate Granger causality analysis of resting-state fMRI. *Neuroimage* 54, 2683–2694.
- Logothetis, N., 2008. What we can do and what we cannot do with fMRI. *Nature* 453, 869–878.
- Marinazzo, D., Liao, W., Pellicoro, M., Stramaglia, S., 2010. Grouping time series by pairwise measures of redundancy. *Physics Letters A* 374, 4040–4044.
- Marinazzo, D., Pellicoro, M., Stramaglia, S., 2012. Causal information approach to partial conditioning in multivariate data sets. *Computational and Mathematical Methods in Medicine* 2012, 8.
- Marrelec, G., Benali, H., Ciuciu, P., Péligrini-Issac, M., Poline, J., 2003. Robust bayesian estimation of the hemodynamic response function in event-related bold fMRI using basic physiological information. *Human Brain Mapping* 19, 1–17.

- Petridou, N., Gaudes, C., Dryden, I., Francis, S., Gowland, P., 2012. Periods of rest in fMRI contain individual spontaneous events which are related to slowly fluctuating spontaneous activity. *Human Brain Mapping*, in press (DOI: 10.1002/hbm.21513).
- Riera, J., Watanabe, J., Kazuki, I., Naoki, M., Aubert, E., Ozaki, T., Kawashima, R., 2004. A state-space model of the hemodynamic approach: nonlinear filtering of bold signals. *NeuroImage* 21, 547–567.
- Roebroeck, A., Formisano, E., Goebel, R., 2005. Mapping directed influence over the brain using Granger causality and fMRI. *Neuroimage* 25, 230–242.
- Roebroeck, A., Formisano, E., Goebel, R., 2011. The identification of interacting networks in the brain using fMRI: model selection, causality and deconvolution. *Neuroimage* 58, 296 – 302.
- Rubinov, M., Sporns, O., 2010. Complex network measures of brain connectivity: uses and interpretations. *Neuroimage* 52, 1059–1069.
- Ryali, S., Supekar, K., Chen, T., Menon, V., 2011. Multivariate dynamical systems models for estimating causal interactions in fMRI. *Neuroimage* 54, 807–823.
- Salvador, R., Suckling, J., Coleman, M., Pickard, J., Menon, D., Bullmore, E., 2005. Neurophysiological architecture of functional magnetic resonance images of human brain. *Cerebral Cortex* 15, 1332–1342.
- Smith, S., Miller, K., Salimi-Khorshidi, G., Webster, M., Beckmann, C., Nichols, T., Ramsey, J., Woolrich, M., 2011. Network modelling methods for fMRI. *Neuroimage* 54, 875–891.
- Stephan, K.E., Roebroeck, A., 2012. A short history of causal modeling of fMRI data. *NeuroImage* 62, 856–863.
- Supekar, K., Menon, V., 2012. Developmental maturation of dynamic causal control signals in higher-order cognition: A neurocognitive network model. *PLoS Computational Biology* 8, e1002374.
- Tagliazucchi, E., Balenzuela, P., Fraiman, D., Chialvo, D., 2012. Criticality in large-scale brain fMRI dynamics unveiled by a novel point process analysis. *Frontiers in Physiology* 3.

- Valdes-Sosa, P., Roebroeck, A., Daunizeau, J., Friston, K., 2011. Effective connectivity: Influence, causality and biophysical modeling. *Neuroimage* 58, 339 – 361.
- Wang, J., Wang, L., Zang, Y., Yang, H., Tang, H., Gong, Q., Chen, Z., Zhu, C., He, Y., 2009. Parcellation-dependent small-world brain functional networks: A resting-state fMRI study. *Human Brain Mapping* 30, 1511–1523.
- Wen, W., Zhu, W., He, Y., Kochan, N., Reppermund, S., Slavin, M., Brodaty, H., Crawford, J., Xia, A., Sachdev, P., 2011. Discrete neuroanatomical networks are associated with specific cognitive abilities in old age. *The Journal of Neuroscience* 31, 1204–1212.
- Wig, G., Schlaggar, B., Petersen, S., 2011. Concepts and principles in the analysis of brain networks. *Annals of the New York Academy of Sciences* 1224, 126–146.
- Zalesky, A., Fornito, A., Harding, I., Cocchi, L., Yücel, M., Pantelis, C., Bullmore, E., 2010. Whole-brain anatomical networks: Does the choice of nodes matter? *Neuroimage* 50, 970–983.
- Zhang, Z., Liao, W., Chen, H., Mantini, D., Ding, J., Xu, Q., Wang, Z., Yuan, C., Chen, G., Jiao, Q., et al., 2011. Altered functional–structural coupling of large-scale brain networks in idiopathic generalized epilepsy. *Brain* 134, 2912–2928.